RSC Publishing Faraday Discussions

FDCDU15 - Carbon Dioxide Utilisation: Novel process and catalytic materials for converting of CO2 and H2 containing mixtures to liquid fuels

Journal:	*Faraday Discussions*
Manuscript ID:	FD-ART-04-2015-000039.R1
Article Type:	Paper
Date Submitted by the Author:	24-Jun-2015
Complete List of Authors:	Meiri, Nora; Ben-Gurion University of the Negev, Dinburg, Yakov; Ben-Gurion University of the Negev, Amoyal, Meital; Ben-Gurion University of the Negev, Koukouliev, Viatcheslav; Ben-Gurion University of the Negev, Vidruk, Roxana; Ben-Gurion University of the Negev, Landau, Miron; Ben-Gurion University of the Negev, Herskowitz, Moti; Ben-Gurion University of the Negev,

Novel process and catalytic materials for converting of CO_2 and H_2 containing mixtures to liquid fuels and chemicals

Nora Meiri, Yakov Dinburg, Meital Amoyal, Viatcheslav Koukouliev, Roxana Vidruk Nehemya, MironV.Landau, Moti Herskowitz*

Chemical Engineering Department, Blechner Center for Industrial Catalysis and Process Development, Ben-Gurion University of the Negev, Beer-Sheva, 84105, Israel

*Corresponding author. Tel.: +972 8 6461482; fax: +972 8 6479427.
E-mail addresses: herskow@bgu.ac.il (M. Herskowitz).

Carbon dioxide and water are renewable and the most abundant feedstock for production of chemicals and fungible fuels. However, the current technologies for production of hydrogen from water are not competitive. Therefore, reacting carbon dioxide with hydrogen is not economically viable in the near future. Other alternatives include natural gas, biogas or biomass for production of carbon dioxide, hydrogen and carbon monoxide mixtures that react to yield chemicals and fungible fuels. The latter process requires a high performance catalyst that enhances the reverse water-gas-shift (RWGS) reaction and Fischer-Tropsch synthesis (FTS) to higher hydrocarbons combined with an optimal reactors system. Important aspects of a novel catalyst, based on a Fe spinel and a three-reactor system developed for this purpose published in our recent paper and patent were investigated in this study. Potassium was found to be a key promoter that improves the reaction rates of RWGS and FTS and increases selectivity to higher hydrocarbons while producing mostly olefins. It changed the texture of the catalyst, stabilized the Fe-Al-O spinel thus preventing decomposition into Fe_3O_4 and Al_2O_3, increased the content of Fe_5C_2 while shifting Fe in the oxide and carbide phases to a more reduced state and the relative exposure of carbide iron on the catalysts surface and increased the CO_2 adsorption and adsorption strength. A detailed kinetic model of the RWGS, FTS and methanation reactions was developed for the Fe spinel catalyst based on extensive experimental data measured over a range of operating conditions. Significant oligomerization activity of the catalyst was found. Testing the pelletized catalyst with CO_2, CO and H_2 mixtures over a range of operating conditions demonstrated its high productivity to higher hydrocarbons. The composition of the liquid (C_{5+}) was found to be a function of the potassium content and the composition of the feedstock.

1. Introduction

Crude oil is the dominant feedstock for production of liquid fuels, as clearly stressed in a recent IEA report[1]. Most of the foreseen output rise over the next three decades will be produced in the Middle East. Biofuels share is currently only 8%, expected to remain at this level until 2040, supported by increasing subsidies. The IEA report sends a very strong message regarding the CO_2 emissions, expected to increase dramatically, unless low-carbon investments will increase by a factor of four

beyond current values. All those projections indicate that the search for alternative, renewable and sustainable sources for production of fungible and competitive fuels needs to be accelerated. Biomass has been the main source for renewable fuels, mainly ethanol and biodiesel. A fierce debate related to future use of biomass has been conducted over the past decade. A recent report[2] presents a less optimistic view of the future of bioenergy in Germany concluding that with the exception of the use of biogenic waste, the larger scale use of biomass as energy source is limited. Proper assessment of the impact of biofuels is critical[3].

Liquid fuels are mixtures of hydrocarbons that meet specific standards updated from time to time. Carbon dioxide, an environmentally damaging greenhouse gas, and water are the most abundant and low-cost sources of carbon and hydrogen needed for production of hydrocarbons. The current scientific and technological challenge is to develop and implement environmentally-friendly processes that convert CO_2 and H_2O into commercially-viable, fungible and compatible fuels, using green energy. A viable route is the reaction of captured carbon dioxide from flue gases with hydrogen produced from water. Methods for both CO_2 capture and water splitting have been recently reviewed[4].

Solar water splitting using photoelectrochemical cells, called artificial photosynthesis has been extensively studied, aimed at developing efficient, robust and scalable processes for production of low-cost, commercially-competitive hydrogen[5-8]. In spite of the extensive scientific effort to provide innovative solutions, the question raised in a recent publication[8] "Will Solar-Driven Water-Splitting Devices See the Light of Day?" remains open. The solar thermochemical cycle method is another promising route being pursued, although no large scale facilities have been developed[9]. Actually the only commercially-proven technology and operated at large scale for water splitting is electrolysis[10]. The cost of hydrogen produced by this method depends mainly on the cost of electricity, estimated to be ~$3/kg at the electricity cost of <$0.055/kWh. This is by far higher than the cost of hydrogen[11] (~$1/kg) produced using the dominant commercial technology, steam reforming of natural gas. The projected cost of hydrogen[11] produced by other water splitting methods is also significantly higher ($3.5/kg - $10/kg).

An economic analysis[12] of the production of liquid solar fuels from carbon dioxide and water was reviewed recently. Employing a modified Fischer-Tropsch process for reacting captured carbon dioxide from flue gas with hydrogen produced by electrolysis for water (using electricity from wind energy) yielded an estimated cost of $5.25/gal of gasoline. The relative high cost of the fuel resulted from the high cost of hydrogen. Another study[13] reviewed sustainable hydrocarbon fuels production by recycling CO_2 and H_2O with renewable or nuclear energy concluded that $3/gal gasoline could be achieved at electricity cost of $0.04-0.05/kWh. The significantly different production cost of the fuels estimated by the two studies results from the different assumptions made in estimating the cost of the electrolysis and the Fischer-Tropsch processes.

A recent paper[14] reviews the catalytic CO_2 hydrogenation to hydrocarbons and describes a novel Fe spinel catalyst coupled with a system of three packed-bed reactors in series with interim removal of water and condensed hydrocarbons that reached a CO_2 conversion of 89% and C_{5+} hydrocarbons productivity of >0.5 kg/kg cat/h. The pure-spinel catalyst displayed a significantly higher activity and selectivity than the other Fe catalysts published in the literature. This process produces hydrocarbons mixtures that can readily be converted to liquid fuels.

Although the CO_2 hydrogenation process is a very promising route to renewable and fungible fuels, its implementation is limited by the availability of low-cost hydrogen produced from water. Only specific locations with access to extremely low-cost electricity (<$0.03/kWh) will operate such competitive processes unless a significantly higher-cost fuel is acceptable for specific purposes like military use. Therefore, other sources of hydrogen should be sought like fossil natural gas or renewable biogas or biomass. Natural gas has been applied commercially[15] as feedstock for production of fuels through conversion to syngas followed by the Fischer-Tropsch synthesis (FTS). The syngas is generated by steam reforming, partial oxidation and autothermal reforming that produce a mixture of hydrogen and carbon monoxide at a molar ratio close to 2. Carbon dioxide generated in those processes is normally separated because it could be detrimental to selectivity or at best is a diluent. Biomass is a potential renewable feedstock for gasification to syngas, containing CO, CO_2 and H_2, which is fed to the FT process. Comprehensive reviews[16,17] describes the potential catalysts, effect of impurities, the economics and the challenges of such processes. A comparison of several routes for production of fuels from biomass, carbon dioxide and electricity[18] based on economical evaluation indicated that the thermochemical route (gasification and conversion to fuels) is by far the preferred route. Biogas is another renewable feedstock that can be readily converted to syngas. This syngas contains a significant amount of CO_2, as pointed out in a recent review[19]. Therefore, the development of suitable FT catalysts that handle mixtures of CO_2, CO and H_2 and are the basis for environmentally-acceptable and competitive processes is a major challenge.

Iron-based catalysts[20,21] that display significant reverse water gas shift (RWGS) activity are employed in processes for converting CO, CO_2 and H_2 mixtures to fuels and chemicals. Specifically, a recent paper[20] discusses the K/Fe−Cu−Al catalyst performance along with carbon deposition by variation of the CO_2/CO ratios. The authors report that in experiments operated for 40 h at 300ºC, 20 bar, CO_2:CO:H_2 molar ratio of 1:1:7 and weight hourly space velocity (WHSV) of the carbon oxides of about 0.83 h^{-1}, the conversion of CO was 96% while the conversion of CO_2 was only 12%. The selectivity to methane was about 10% while the selectivity to C_{5+} was about 60%. The significant conclusion of this study was that operating at a high $CO_2/(CO + CO_2)$ ratio and high pressure and temperature prevents carbon deposition on the Fe-based catalyst. A recent patent[22] extends the information on the novel catalytic system[14] from mixtures of CO_2 and H_2 to CO_2, CO and H_2 mixtures.

Potassium was identified as an important component of the Fe-based catalysts for the FTS. In a recent review[23], the authors concluded that the presence of potassium reduces the formation of CH_4 while increasing the selectivity to higher hydrocarbons. A similar effect was reported in an early study[24] of CO_2 hydrogenation. This effect was related to the enhanced carburization of the Fe catalyst in the presence of potassium. A recent study[25] reported the effect of potassium on the CO_2 in the hydrogenation of mixtures of CO and CO_2. Apparently, increasing the K content did not increase the catalyst activity while the average product molecular weight increased.

It is generally accepted that K acts as electronic promoter when adsorbed at the surface of $Fe^o/FeO_x/FeC_x$ phases particles lowering the iron work function due to interaction between alkali metal valence state and conduction band states in catalytic phases[26,27]. Donating electron density to the vacant d-orbital of iron enhances the dissociative adsorption of CO while lowering the H_2 adsorption ability[27]. Depressing hydrogenation activity is associated with lower rates of CH_4 formation, higher selectivity to olefins and long-chain hydrocarbons. The oxidative action of CO_2 and excessive water on Fe-carbide phases[28] during CO_2 hydrogenation creates more oxidized iron on the catalysts that may modify the action of the K promotor.

The hydrogenation of mixtures of CO and CO_2 is a complex process that requires optimization through modeling and simulations. A recent study[29] describes the simulation that includes steam reforming of natural gas with addition of CO_2. The FTS was simulated using experimental results previously published[20] by the authors. While numerous kinetic models have been proposed for Fe-based FT catalysts, limited information was published on the kinetic behavior of catalysts for the hydrogenation of CO_2. A kinetic study[30] of CO_2 hydrogenation proposed two rates expressions, one for reverse WGS and the other for the FT. The experiments were conducted at 10 bar and stoichiometric H_2/CO_2 ratio of 3. The highest measured CO_2 conversion was 45% at 300ºC to 60% at 400ºC due to the equilibrium limitation of the reverse WGS. Another kinetic study[31] was conducted at high H_2/CO_2 molar ratios of 4 and 8 that produced a light product (α = 0.2-0.3). A similar kinetic model that included two reactions (reverse WGS and FT) was used. The highest CO_2 conversion was 44% at H_2/CO_2 molar ratio of 8. Increasing temperature and residence time did not increase the conversion.

A more detailed kinetic study of FTS on $K/Fe–Cu–Mn–Al_2O_3$ catalysts has been published[32]. It includes 10 reactions of CO and H_2, nine of them to light paraffins (C_1-C_4) and olefins (C_2-C_4). The last reaction represents the production of C_{5+} hydrocarbons lumped in one component C_6H_{14}. The selection of hexane means that the liquid product was very light and mostly paraffinic. No oxygenates were mentioned in this study.

Potential applications of catalytic processes for converting mixtures of CO_2, CO and H_2 to hydrocarbons and oxygenates to be readily converted to liquid fuels and chemicals requires sustained research aimed at improving the performance of the catalysts (selectivity to higher hydrocarbons and

olefins, activity and stability) and optimization of the processes. One of the most important components of Fe-based catalysts is potassium. Developing a better understanding of the effects of potassium as promoter is a key factor in improving performance. Optimization of the process requires a reliable kinetic model to be implemented in modeling and simulations. The scope of this study is to determine some of the fundamental effects of potassium of the Fe spinel catalyst, to develop a detailed kinetic model of the CO_2 hydrogenation on the Fe spinel catalyst and present effects of the feed composition and operating conditions on the performance of the pelletized Fe spinel catalyst in a fixed bed reactor.

2. Experimental

Catalysts preparation

The K-promoted, pure Fe–Al–O spinel $Fe(Fe_{0.5}Al_{0.5})_2O_4$ catalyst used in this study was prepared and characterized according to procedures described elsewhere[14]. Potassium was added to the dried Fe-Al-O spinel precursor by incipient wetness impregnation with an aqueous solution of K_2CO_3, followed by overnight drying at 110°C and calcination in air at 450ºC for 6 h. Three Fe-based spinel catalysts with different K content were prepared: unpromoted 100Spinel/0wt% K (Cat.Fe-0K), 100Spinel/2wt% K (Cat.Fe-2K) and 100Spinel/4wt% K (Cat.Fe-4K).

Catalysts characterization

The spent catalysts were characterized after He treating and passivation. After testing, the catalysts were treated in He flow at 300°C for 3 h for removal of residual adsorbed organics and passivated in CO_2 flow at 25ºC for 1 h. The textural properties of the catalysts, surface area, pore volume and pore size, were calculated from N_2 adsorption-desorption isotherms using conventional BET and BJH methods. The isotherms were recorded on a NOVA 3200e (Quantachrome) at the temperature of liquid nitrogen after degasing in vacuum at 100ºC. The phase composition of the catalysts was determined based on their X-ray diffraction patterns. XRD measurements were conducted at the Phillips 1050/70 powder diffractometer fitted with graphite monochromator, at 40 kV and 28 mA using software developed by Crystal logic. The phase identification was performed by using a SBDE ZDS computer search/match program coupled with the ICDD. The relative content of iron oxide and carbide phases was obtained by Rietveld refinement of the XRD profile by using the DBWS-9807 program. The elemental composition of the catalysts was measured by the EDS method (Quanta-200, SEM-EDAX, FEI Co instrument). The CO_2-TPD measurements were performed using Chemisorption Analyzer Autochem II 2920 instrument, Micrometrics Co. The samples were saturated with CO_2 at 40ºC before recording the desorption spectra with a heating rate 5ºC min^{-1} in 5%CO_2/He flow of 25 ml min^{-1}. XPS data were collected using X-ray photoelectron spectrometer ESCALAB 250 ultrahigh vacuum ($1x10^{-9}$ bar) apparatus with an Al Kα X-ray source and a monochromator. The spectral components of C and Fe signals were found by fitting a sum of single component lines to the experimental data by means of non-

linear least-square curve fitting. The EX05 argon gun system performed controlled removal of surface layers allowing the depth profile analyses of elements.

Catalysts performance testing

Measurements of the catalysts activity and selectivity including data for the kinetic model were carried out in two units:

1. A computer-controlled bench rig equipped with three continuous-flow fixed bed reactors connected in series including devices for removing water and organic liquid between reactors[14] for the kinetic runs (packed with 50 – 200 µm powder) and CO_2, CO and H_2 mixtures (packed with 1.4-1.7 mm pellets) runs. The pellets were prepared by pressing the powder catalyst. The catalyst was mixed with silica powder diluent and packed in the reactors.
2. One fixed-bed reactor packed with diluted (silica) powder catalyst followed by a cooler and a gas-liquid separator for studying the effect of potassium.

The hydrocarbon liquid mixture and oxygenates from aqueous products were separated and analyzed by GC-MS (Agilent Technologies 6890N network GC system equipped with 5973 Network mass-selective detector). CO_2, H_2, CO and C_1-C_6 hydrocarbons were analyzed on line using GC instrument Agilent Technologies, model 7890A equipped with 5 valves / 7 columns (PLOT and packed)/2 TCD/ FID detectors. The organics content in aqueous product was measured by TOC analysis (instrument TOC-V_{CPN} Shimadzu Co.).

3. Results and Discussion

3.1 Effects of potassium as promoter of the Fe-spinel catalyst

The catalysts were activated in situ by H_2/CO carburization with a stream of 0.03:0.03:0.14 NmL min^{-1} g^{-1}_{cat} of CO, H_2 and He, respectively, at 300°C for 3 h. The catalysts were tested at constant conditions of 20 bar, 320°C and H_2/CO_2 molar ratio of 3. The WHSV of CO_2 was adjusted to reach about 30% CO_2 conversion so as to achieve differential operation of the reactor and calculate directly the reaction rates. The catalysts reached steady state yielding constant CO_2 conversion / products selectivity after 120 h on stream. After the end of the run, the catalysts were treated with He and then passivated with CO_2 before discharged from the reactor.

Effect of potassium on the performance of Fe-Al-O spinel catalyst in CO_2 hydrogenation

The performance measured with the three catalysts, Cat.Fe-0K, Cat.Fe-2K and Cat.Fe-4K, listed in Table 1 demonstrates a significant effect of potassium on the catalyst activity and selectivity. The RWGS rate of reaction was calculated from the differential measurements of the CO_2 conversion (30%) and WHSV. The rate of methanation was calculated from the molar flow rate of methane and the

catalyst weight. Similarly, the rate of FTS reaction was calculated from the molar flow rate of all hydrocarbons (without methane) and oxygenates and the catalyst weight.

Adding 2 wt% potassium increased dramatically both the RWGS and FTS rates of reaction and decreased the rate of methanation. Further increasing the potassium content decreased the reaction rate of RWGS. The methanation rate displayed an extreme drop thus increasing the selectivity of the desired products. The FTS reaction rate decreased mildly. Actually, the ratio of the FTS/RWGS reaction rates increased gradually as the potassium content increased which has a very important impact on the process. The effect of potassium on selectivity was very impressive and dominant. Beyond the drop in the methane selectivity, the significant increase in the selectivity to higher hydrocarbons (C_{5+}) is a substantial factor. Those findings are in agreement with the results presented in other studies of Fe-catalysts in CO and CO_2 hydrogenation[23,33].

Table 1 Effect of potassium on the performance of Fe-Al-O spinel catalyst in CO_2 hydrogenation
Testing conditions: 20 bar, 320°C, molar $H_2/CO_2 = 3$, 120 h on stream

Catalyst	**Reactions rates, mmol $g_{cat}^{-1}h^{-1}$**				**Products selectivity, wt%**					
	RWGS	**FTS**	**CH_4**	**FTS/ RWGS**	**CO**	**CH_4**	**C_2-C_4**			**C_{5+}**
							Olefins	Paraffins	Oxygenates	
Cat.Fe-0K	125	62	46	0.50	15	40	15	15	8	7
Cat.Fe-2K	179	112	34	0.63	22	23	24	11	4	16
Cat.Fe-4K	123	95	6	0.77	22	6	24	5	10	33

Effect of potassium on the texture, chemical/ phase composition and surface chemistry of Fe-Al-O spinel

The texture measurements of the spent catalysts after operation of 120 h listed in Table 2 indicate a significant decrease of the surface area, pore volume and diameter as potassium content increased. This may be attributed to increasing crystal size or aggregation of nanoparticles of the Fe-oxide and carbide phases produced from Fe-Al-O spinel during activation and self-organization in presence of K as was observed in[34] for other Fe-catalysts. It may also be attributed to the blocking of pores with coke or wax which was increasingly deposited as the potassium content increased.

Table 2 Effect of potassium on the texture parameters of Fe-Al-O spinel spent catalysts
Testing conditions: 20 bar, 320°C, molar H_2/CO_2 = 3, 120 h on stream

Catalyst	Surface area, $m^2 g^{-1}$	Pore volume, $cm^3 g^{-1}$	Average pore diameter, nm
Cat.Fe-0K	78	0.23	6.0
Cat.Fe-2K	55	0.16	5.6
Cat.Fe-4K	42	0.10	4.6

The chemical composition of spent catalysts expressed as the weight ratio related to Fe is shown in Table 3. The catalyst containing 2 wt% K accumulated about the same amount of total carbon as the catalyst with no K. Increasing the amount of potassium to 4 wt% increased the total carbon content from 0.23 to 0.42. In all cases, the atomic ratio C/Fe was greater than unity, much higher than in any of iron carbide phases FeC_x stable at testing conditions (i.e. Fe_5C_2, Fe_7C_3). It means that the spent catalysts contained a significant amount of coke or wax carbon deposited during self-organization.

Table 3 Chemical composition of Fe-Al-O spinel spent catalysts
Testing conditions: 20 bar, 320°C, molar H_2/CO_2 = 3, 120 h on stream

Catalyst	Chemical composition							
	wt ratio				Atomic ratio			
	Fe	Al	C	K	Fe	Al	C	K
Cat.Fe-0K	1	0.21	0.25	0.0	1	0.44	1.2	0.0
Cat.Fe-2K	1	0.22	0.23	0.05	1	0.45	1.1	0.08
Cat.Fe-4K	1	0.20	0.42	0.10	1	0.42	1.9	0.13

The quantitative XRD phase analysis revealed a strong effect of potassium promoter on the phase composition of the spent catalysts as illustrated by the results listed in Table 4. The calculations of the phases content and their average crystal size were conducted based on their X-ray diffraction patterns shown in Fig. 1. All catalysts contain two Fe-carbide phases: χ- Fe_5C_2 and Fe_7C_3 formed as a result of spinel activation and self-organization when part of iron was removed from the spinel phase. This decreases the x value in the formula of spinel phase $Fe^{II}[(Fe^{III}_xAl_{1-x})_2]O_4$ from 0.5, in fresh catalyst, to 0.2 - 0.3 in Fe-poor spinel residua measured according to the positions of characteristic reflections in X-ray diffractograms.

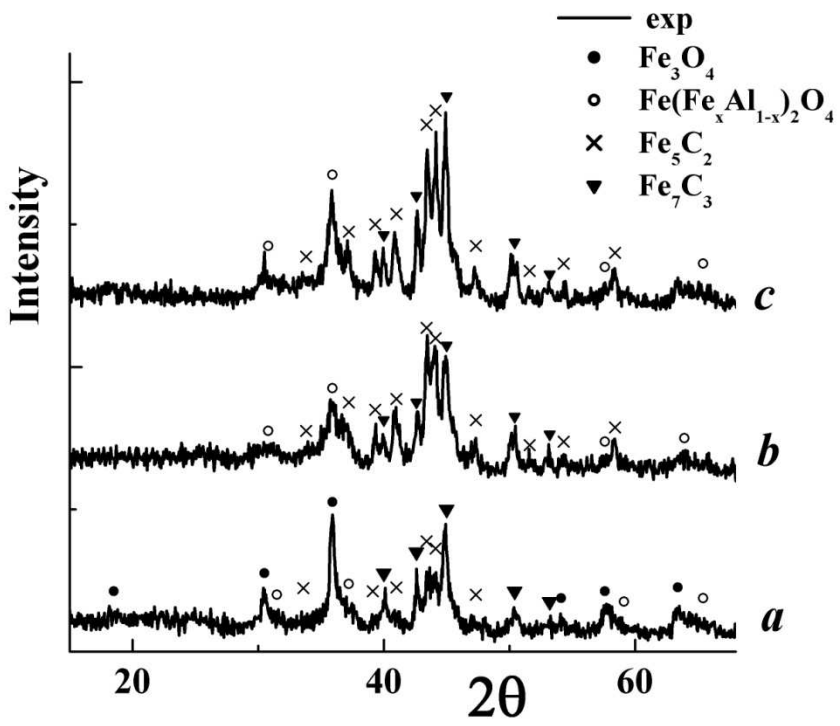

Fig. 1.XRD patterns of Fe-Al-O spinel catalyst after reaching steady state in catalytic testing run. (a) "Cat.Fe-0K", (b) "Cat.Fe-2K", (c) "Cat.Fe-4K". Testing conditions: P= 20 bar, T= 320°C, H_2/CO_2=3, 120 h on stream

Table 4 Phase composition of Fe-Al-O spinel spent catalysts
Testing conditions: 20 bar, 320°C, molar H_2/CO_2 = 3, 120 h on stream

Catalyst	**Spinel wt%**	**Crystal size, nm**	**Magnetite wt%**	**Crystal size, nm**	**χ- Fe_5C_2 wt%**	**Crystal size, nm**	**Fe_7C_3 wt%**	**Crystal size, nm**	**χ- Fe_5C_2/ (χ-Fe_5C_2+ Fe_7C_3)**
Cat.Fe-0K	27	8	18	35	34	25	21	35	62
Cat.Fe-2K	41	5	0	-	47	30	12	40	80
Cat.Fe-4K	42	6	0	-	42	35	16	40	72

A very significant result is the removal of Fe from Fe-Al-O spinel in catalyst Cat.Fe-0K that was partially decomposed into Fe-poor spinel (27 wt%), amorphous alumina whose reflections cannot be observed in the diffractogram and magnetite (18 wt%). Adding potassium prevents the formation of magnetite phase while the content of Fe-poor spinel increased to 41-42 wt%. Potassium also enhances carburization of the Fe-Al-O spinel precursor to the active χ- Fe_5C_2 phase[35]. Interestingly, the content of χ- Fe_5C_2 phase decreased as the potassium content increased from 2 wt% to 4 wt%. A relatively little

change in the crystal size of the two iron carbide phases in two potassium promoted catalysts was observed.

The XPS spectra of the spent unpromoted and K-promoted Fe-Al-O spinel catalysts, as-received and after Ar-etching, are shown in Fig. 2 and 3. The BE for detected peaks and surface concentrations of corresponding atoms are given in Tables 5 and 6. Two main peaks were detected in the XPS spectra of iron. The first is attributed to the iron carbides at lower binding energy around 707.1-707.5 eV corresponding to near-metallic state of iron and the second belongs to iron ions in oxide phases with higher binding energy in the range of 710.4.5-711.5 eV. The latter peaks represent superposition of signals contributed by Fe^{2+} with BE of 709.5 and of Fe^{3+} with BE of 711.2 eV[36,37]. Insertion of 2 wt% potassium shifted the BE of carbide and oxide iron atoms to lower values: from 707.5 (707.4 after etching) to 707.3 eV and from 711.5 (710.8 after etching) to 710.8 (710.4 after etching) eV. This corresponds to formation of more reduced states of iron in carbides and in Fe-poor spinel due to electron-donation of K-promoter[26,27].

Table 5 Binding energies and concentrations of surface atoms Fe-Al-O spinel spent catalyst
Testing conditions: 20 bar, 320°C, molar $H_2/CO_2 = 3$, 120 h on stream

Catalyst name	**C 1S core**		**Fe 2P $_{3/2}$ core**		
	BE, eV	**% Atomic**	**BE, eV**	**% Atomic**	**Fe_{carb}/Fe_{ox}**
Cat.Fe-0K	284.3	11	707.5	4	0.04
	284.8	31			
	285.5	19	711.5	96	
	286.5	17			
	288.6	22			
Cat.Fe-2K	284.1	18	707.3	10	0.11
	284.8	48	710.8	90	
	285.4	34			
Cat.Fe-4K	284.0	19	707.1	11	0.12
	285.1	55	710.7	89	
	286.3	26			

Table 6 Binding energies and concentrations of surface atoms Ar-etched Fe-Al-O spinel spent catalyst
Testing conditions: 20 bar, 320°C, molar H_2/CO_2 = 3, 120 h on stream

Catalyst	C 1S core		Fe 2P $_{3/2}$ core		
	BE, eV	% Atomic	BE, eV	% Atomic	Fe_{carb}/Fe_{ox}
Cat.Fe-0K	284.3	26	707.4	23	0.30
	284.8	36	710.8	77	
	285.6	39			
Cat.Fe-2K	283.6	16	707.3	36	0.56
	284.8	53	710.4	64	
	285.5	31			
Cat.Fe-4K	284.0	19	707.5	34	0.52
	285.1	55	710.8	66	
	286.3	26			

Insertion of K increased the surface concentration or relative exposure of carbide iron. Deconvolution of XPS envelops recorded for C 1S core show the coexistence of three groups of signals: peaks with BE 283.6-284.3 eV corresponding to Fe-carbide carbon, 284.8-285.1 eV belonging to C-C sp^2 and sp^3 in carbon and hydrocarbons (-CH_2=CH) deposits and 285.4-288.6 eV characteristic for adsorbed carbon oxygenates moieties containing C=O, C-O, CH_2-O, O-C=O and other oxygen groups[36,38,39]. Insertion of potassium increases the relative exposure of carbide carbon at the spent catalysts surface (from 11 to 19%). This is in agreement with growing of the exposure of carbide iron. Potassium also significantly increases the relative exposure of carbon belonging to graphite and hydrocarbons deposits from 31% (36% after etching) in the unpromoted catalyst to 48-55% in the catalysts containing 2-4wt% K. At the same time insertion of potassium removes the oxygenated moieties with high C 1S BE from 58% (39% after etching) in the unpromoted catalyst to 26-34% in the K-promoted catalysts.

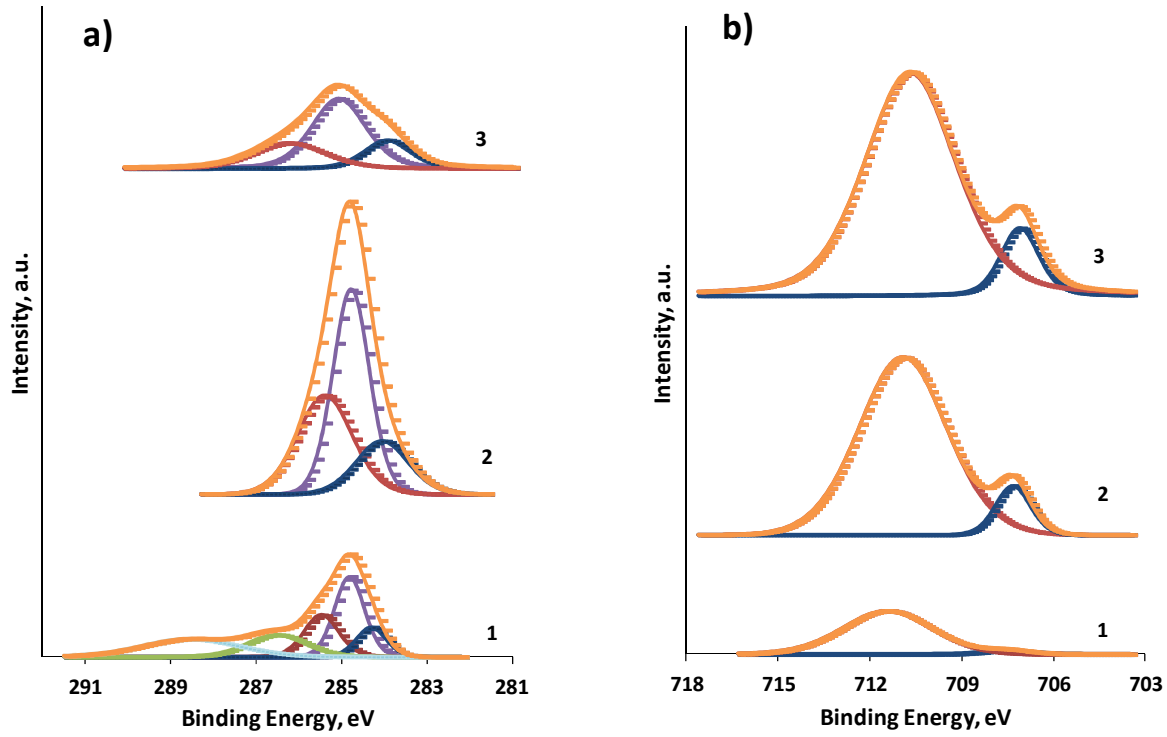

Fig. 2. XPS spectra recorded with as-received spent Fe-Al-O spinel catalysts : a) – C 1S core; b) – $Fe_{3/2}$ core: 1 – unpromoted catalyst; 2 – 2 wt%K; 3 – 4 wt% K

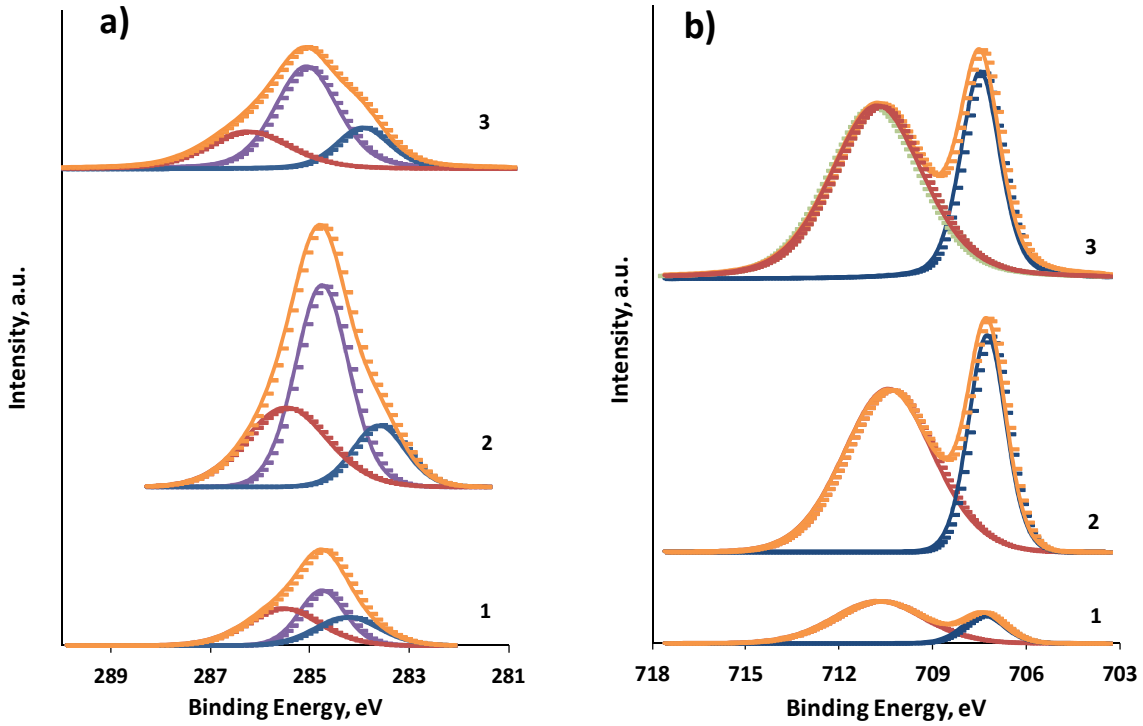

Fig. 3. XPS spectra recorded with spent Fe-Al-O spinel catalysts after Ar-etching: a) – C 1S core; b) – $Fe_{3/2}$ core: 1 – unpromoted catalyst; 2 – 2 wt% K; 3 – 4 wt% K.

Potassium is expected to increase the basicity of Fe-Al-O spinel thus increasing the surface coverage with acidic CO_2 reagent molecules. The CO_2-TPD spectra illustrated in Fig. 4 indicate that the 2 wt% K catalysts displayed one CO_2 desorption peak centered at ~150^{o}C which represent relatively weak surface basic sites. Increasing of K content to 4 wt% further increased the weak basicity by a factor of 2.5. Furthermore, at high K content of 4 wt% appeared two additional CO_2 desorption peaks centered at 550 and 850^{o}C, corresponding to very strong basic sites. These results may be explained assuming strong interaction between Fe-Al-O spinel and potassium. At low concentrations of K, it mainly stabilizes the Fe-Al-O spinel phase, as detected by XRD. But at high concentration of 4 wt%, potassium may exist in a free form of adsorbed K_2O, displaying strong surface basicity.

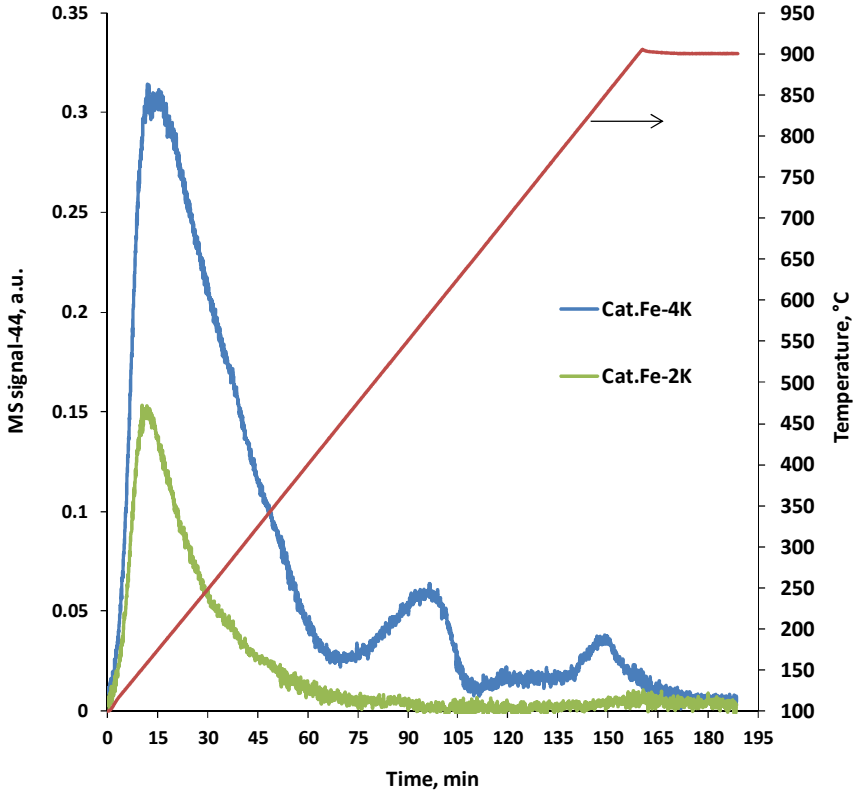

Fig. 4. CO_2-TPD spectra recoded with fresh K/Fe-Al-O spinel catalysts

3.2 Kinetic model

Kinetic data were measured for the 4 wt% spinel Fe catalyst in a three-reactors-in-series system over a range of operating conditions (300-340ºC, 20-28 bar, molar H_2/CO_2 = 2.9, WHSV = 1-6 h^{-1}). In essence two processes took place in series: RWGS and FTS. Oligomerization of light olefins was also found to be important. In contrast to the recent kinetic model[32] that employed power law expressions for all 10 reaction rates of FTS, our model consists of LHHW (Langmuir-Hinshelwood-Hougen-Watson) expressions that include an adsorption term in the denominator. This term contains two components: H_2O and CO_2. The reactions were selected so as to reflect the main findings of the kinetic study: the

RWGS reaction, methanation reaction, 7 FTS reactions and 4 oligomerization reactions. The 7 FT reactions (3-9) produce light paraffins (C_2-C_5), four light olefins (C_2, C_3, C_4 and C_5), C_{6+} represented by decene and oxygenates represented by butanoic acid. The oligomerization reactions (10-13) convert the light olefins to C_{6+} products represented by decene. The reactions are listed in Table 7. The mass balances expressed by equation (1) assume plug-flow with no internal or external mass and heat transfer resistances:

$$\frac{d\omega_i}{d\left(\frac{1}{WHSV}\right)} = R_i \cdot \omega_{CO_2,in} \cdot Mw_i \qquad (1)$$

where ω_i is the mass fraction of component i, WHSV is the weight hourly space velocity of CO_2, R_i is the rate of change in the reaction where component i is a reactant/product, $\omega_{CO_2,in}$ is the mass fraction of CO_2 at inlet and Mw_i is the molecular weight of component i.

The kinetic expressions are also listed in Table 7. Kinetic modeling of the experimental data was conducted employing MATLAB, using 216 data points measured at the outlet of the first, second and third reactor. The MATLAB function "ode113" solved the differential equations system. Kinetic models were fitted to the data using "Fmincon" function used to find the minimum SSE value. The kinetic constants, including pre-exponent coefficient and activation energy, are listed in Table 8. The adsorption constants, including the adsorption pre-exponential factor and the heat of adsorption, are listed in Table 9. A parity plot of ω_i of all components at the outlet of each reactor that reflects the good agreement of the experimental data with values calculated with the model (R^2 calculated using regression statistics is 0.99) is depicted in Fig. 5. The predicted and experimental weight fractions of CO_2 and CO at the outlet of each one of the three reactors at 320ºC and 20 and 28 bar, depicted in Fig. 6, are in good agreement. They illustrate the significant contribution of each reactor and the relatively weak effect of total pressure.

Table 7 Key components and reactions and rate expressions of the kinetic model

Comp.	Name	Formula	Comp.	Name	Formula
1	Carbon Dioxide	CO_2	7	Propylene	C_3H_6
2	Hydrogen	H_2	8	Propane*	C_3H_8
3	Carbon Monoxide	CO	9	1-Butene	C_4H_8
4	Water	H_2O	10	Pentene	C_5H_{10}
5	Methane	CH_4	11	Decene**	$C_{10}H_{20}$
6	Ethylene	C_2H_4	12	Butanoic acid***	$C_4H_8O_2$

* C_2-C_5 paraffins; ** C_6+; *** oxygenates

1. $CO_2 + H_2 \leftrightarrow CO + H_2O$ $\qquad r_1 = k_1 \cdot \frac{p_1 \cdot p_2 - \frac{p_3 \cdot p_4}{Keq}}{1+K_4 p_4 + K_1 \cdot p_1}$

2. $CO + 3H_2 \rightarrow CH_4 + H_2O$ $\qquad r_2 = k_2 \cdot \frac{p_3 \cdot p_2^{0.2}}{1+K_4 \cdot p_4 + K_1 \cdot p_1}$

3. $CO + 2H_2 \rightarrow \frac{1}{2}C_2H_4 + H_2O$ $\quad r_3 = k_3 \cdot \frac{p_3 \cdot p_2^{0.2}}{1+K_4 \cdot p_4 + K_1 \cdot p_1}$

4. $CO + 2H_2 \rightarrow \frac{1}{3}C_3H_6 + H_2O$ $\quad r_4 = k_4 \cdot \frac{p_3 \cdot p_2^{0.2}}{1+K_4 \cdot p_4 + K_1 \cdot p_1}$

5. $CO + \frac{7}{3}H_2 \rightarrow \frac{1}{3}C_3H_8 + H_2O$ $\quad r_5 = k_5 \cdot \frac{p_3 \cdot p_2^{0.2}}{1+K_4 \cdot p_4 + K_1 \cdot p_1}$

6. $CO + 2H_2 \rightarrow \frac{1}{4}C_4H_8 + H_2O$ $\quad r_6 = k_6 \cdot \frac{p_3 \cdot p_2^{0.2}}{1+K_4 \cdot p_4 + K_1 \cdot p_1}$

7. $CO + 2H_2 \rightarrow \frac{1}{5}C_5H_{10} + H_2O$ $\quad r_7 = k_7 \cdot \frac{p_3 \cdot p_2^{0.2}}{1+K_4 \cdot p_4 + K_1 \cdot p_1}$

8. $CO + 2H_2 \rightarrow \frac{1}{10}C_{10}H_{20} + H_2O$ $\quad r_8 = k_8 \cdot \frac{p_3 \cdot p_2^{0.2}}{1+K_4 \cdot p_4 + K_1 \cdot p_1}$

9. $CO + \frac{6}{4}H_2 \rightarrow \frac{1}{4}C_4H_8O_2 + \frac{2}{4}H_2O$ $\quad r_9 = k_9 \cdot \frac{p_3 \cdot p_2^{0.2}}{1+K_4 \cdot p_4 + K_1 \cdot p_1}$

10. $C_2H_4 \rightarrow \frac{1}{5}C_{10}H_{20}$ $\quad r_{10} = k_{10} \cdot \frac{p_6^{1.3}}{1+K_4 \cdot p_4 + K_1 \cdot p_1}$

11. $C_3H_6 \rightarrow \frac{1}{3.3}C_{10}H_{20}$ $\quad r_{11} = k_{11} \cdot \frac{p_7^{1.8}}{1+K_4 \cdot p_4 + K_1 \cdot p_1}$

12. $C_4H_8 \rightarrow \frac{1}{2.5}C_{10}H_{20}$ $\quad r_{12} = k_{12} \cdot \frac{p_9^{1.6}}{1+K_4 \cdot p_4 + K_1 \cdot p_1}$

13. $C_5H_{10} \rightarrow \frac{1}{2}C_{10}H_{20}$ $\quad r_{13} = k_{13} \cdot \frac{p_{10}^{1.3}}{1+K_4 \cdot p_4 + K_1 \cdot p_1}$

Table 8 Kinetic constants of the rate expressions

k_j	k_{0j}	Units	E_j, kJ mol^{-1}	k_j	k_{0j}	Units	E_j, kJ mol^{-1}
k_1	5.5E+06	mol g^{-1} h^{-1} MPa^{-2}	72.2	k_8	4.0E+03	mol g^{-1} h^{-1} MPa$^{-1.2}$	33.4
k_2	1.0E+09	mol g^{-1} h^{-1} MPa$^{-1.2}$	98.0	k_9	3.6E+03	mol g^{-1} h^{-1} MPa$^{-1.2}$	31.5
k_3	1.2E+04	mol g^{-1} h^{-1} MPa$^{-1.2}$	45.0	k_{10}	2.7E+03	mol g^{-1} h^{-1} MPa$^{-1.3}$	25.8
k_4	1.2E+05	mol g^{-1} h^{-1} MPa$^{-1.2}$	53.6	k_{11}	1.4E+04	mol g^{-1} h^{-1} MPa$^{-1.8}$	35.5
k_5	1.8E+04	mol g^{-1} h^{-1} MPa$^{-1.2}$	46.4	k_{12}	3.7E+04	mol g^{-1} h^{-1} MPa$^{-1.6}$	40.7
k_6	1.1E+03	mol g^{-1} h^{-1} MPa$^{-1.2}$	31.5	k_{13}	6.0E+07	mol g^{-1} h^{-1} MPa$^{-1.3}$	88.8
k_7	9.0E+02	mol g^{-1} h^{-1} MPa$^{-1.2}$	31.5				

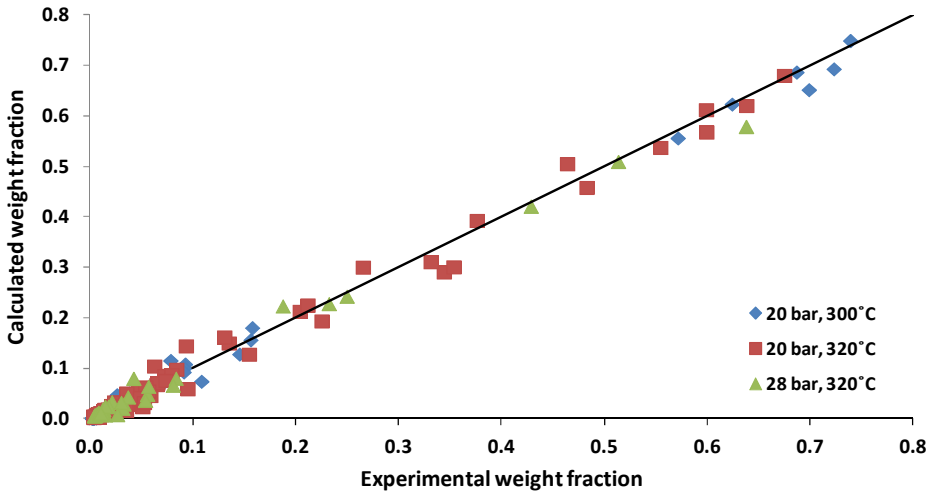

Fig. 5. Parity plot of the calculated and experimental data

Table 9 Adsorption constants of CO_2 and H_2O

K_i	k_{0i},MPa^{-1}	ΔH_{ai},kJ mol^{-1}
K_1	2.1E-02	33.4
K_4	2.4E-02	31.5

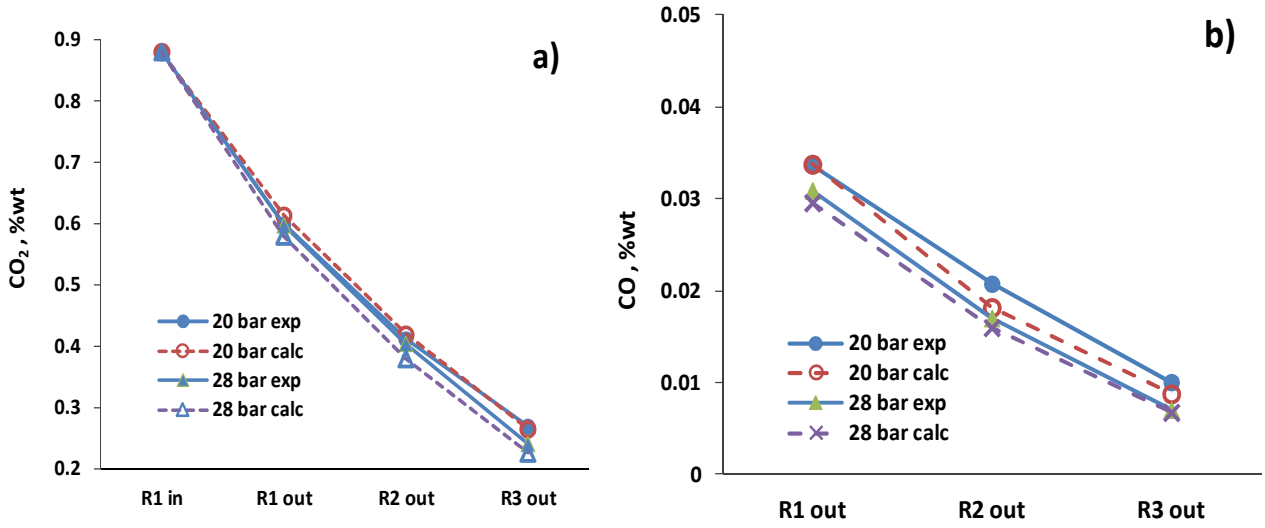

Fig. 6. Calculated vs. experimental weight fraction of CO_2 (a) and CO (b) at the outlet of the three reactors system at molar H_2/CO_2 = 2.9, 320^{o}C, WHSV = 3 h^{-1}

The kinetic developed for the catalyst containing 4 wt% K will be further extended to account for the significant effect of potassium. Furthermore, it will be employed to evaluate the effectiveness factor of the reactions in the model for pelletized catalyst. CO in the process feed will also be examined. This will facilitate the application of the kinetic model to simulate the performance of the process at operating conditions that are relevant to commercial applications.

3.3 Conversion of CO_2, CO and H_2 mixtures to higher hydrocarbons

The process described in this study was conducted with a feed containing CO_2 and H_2 and a mixture that contained CO_2, CO and H_2. The data presented here were measured with pelletized (1.4-1.7 mm) catalysts containing 3 wt% and 4 wt% K over a range of feed compositions and operating conditions to examine the potential of the process at conditions relevant for commercial applications. Furthermore, the data will be employed in the simulations of the process.

Experiments were carried out in the three-reactor system at 20 and 30 bar, 320 and 330°C, over a range of operating conditions, including feed composition and WHSV. The results of 5 runs, 4 of them at 20 bar and run P-63-300 at 30 bar, are listed in Table 10. The oxygenates listed in Table 10 are dissolved in water. The composition of the organic liquid collected in runs P-63-164 and P-65-69 is given in Table 11. WHSV is calculated as mass flow rate of CO_2 and CO divided by the mass of catalyst. The other parameters are defined in Table 10. sCO_x is defined so that a molar $H_2/sCO_x = 1$ is stoichiometric for all feed compositions. The mass balance in all 4 runs was >94%.

Run P-63-164 was carried out with catalyst containing 4 wt% K at 20 bar with stoichiometric feed. The conversion was relatively high and the selectivity to C_{5+} was >50 wt%. P-63-300 was conducted with sub-stoichiometric ratio. Thus the CO_2 conversion was lower than that of H_2. WHSV and the pressure were increased from 1.1 h^{-1} and 20 bar to 1.3 h^{-1} and to 30 bar, respectively. Increasing WHSV should lower the conversion while increasing pressure should increase the conversion. Apparently, the two changes offset each other thus the conversion changed little. The selectivity in the runs is rather similar, although the methane selectivity in run P-63-300 is slightly lower and the C_{5+} selectivity slightly higher.

Introducing CO to the feed in the system packed with catalyst containing 4 wt% K led to a gradual deterioration of the catalyst performance as shown in run P-65 depicted in Table 10. This was rectified in Run P-66 by replacing the catalyst in the first reactor with a 3 wt% K catalyst that displayed stable performance. The performance of two reactors in series, P-66-396 R1 (after one reactor) and R2 (after two reactors) listed in Table 10, indicates that the conversion of CO is much higher than the CO_2 conversion in both reactors. The selectivity in both reactors is similar.

Table 10 Performance of CO_2 and CO hydrogenation process on pelletized catalyst

Run	WHSV h^{-1}	Temp °C	H_2/sCO_x molar	CO_2/CO_x molar	x_1 %	x_2 %	x_3 %	S_4 %	S_5 %	S_6 %	S_7 %	S_8 %	S_9 %	S_{10} %
P-63-164	1.0	320	1.0	1.0	82	81.7	-	10.5	6.2	18.5	2.0	2.7	51.9	8.2
P-63-300	1.3	320	0.9	1.0	77.6	87.9	-	9.6	5.5	15.6	2.1	2.6	54.1	10.5
P-65-45	0.9	330	1.1	0.7	63.8	70.9	92.0	11.6	7.0	19.7	1.8	2.5	49.1	7.9
P-65-69	0.9	330	1.1	0.7	61.6	68.7	90.3	11.3	6.6	17.9	1.8	2.5	51.8	8.1
P-65-93	0.9	330	1.1	0.7	58.6	68.6	90.0	12.0	6.7	18.2	2.0	3.1	50.4	7.8
P-65-141	1.0	330	1.1	0.7	48.3	63.0	83.2	13.8	7.5	12.7	2.4	3.5	50.7	9.8
P-66-396 R1	1.0	320	0.7	0.8	20.6	33.9	48.7	12.9	7.7	22.4	1.9	2.9	45.0	7.2
P-66-396 R2	1.0	320	0.7	0.8	39.0	66.8	86.7	11.1	6.9	21.0	2.3	2.9	47.8	7.9

The reactants are defined as: $CO_2 \equiv A_1$; $H_2 \equiv A_2$; $CO \equiv A_3$ while the products are listed as: $CH_4 \equiv A_4$; $C_2H_4 \equiv A_5$; $C_3H_6+C_4H_8 \equiv A_6$; $C_2H_6 \equiv A_7$; $C_3H_8+C_4H_{10} \equiv A_8$; $C_{5+} \equiv A_9$; oxygenates $\equiv A_{10}$; $H_2O \equiv A_{11}$; $sCO_x = 3*CO_2 + 2*CO$; $CO_x = CO_2 + CO$; x_j is the conversion of reactant j ; S_j is the selectivity of product j expressed as the mass fraction of the carbon converted to that product.

The composition of the organic phase in runs P-63-164 and P-66-396 is listed in Table 11. As expected, the liquid contained much more olefins (>65 wt%) than paraffins (<25 wt%). A comparison of the products distribution between naphtha and distillates in the two experiments and the data measured with the 3 wt% K catalyst published elsewhere[14] is depicted in Fig. 7. Surprisingly, the first reactor packed with 3 wt% K catalyst in run P-66-396 yielded a slightly heavier product compared with the product in the second reactor of the same run and in the three combined reactors in run P-63-164, packed with 4 wt% K catalyst. This is probably due to the fact that the feed to the first reactor contained a significant concentration of CO. Furthermore, the product obtained with a stoichiometric mixture of H_2 and CO_2 in a three-reactor unit packed with a 3 wt% K catalyst[14] yielded a much lighter product than produced with a 4 wt% K catalyst.

Table 11 Composition of the organic liquid in runs P-63-164 and P-66-396

		P-66-396		P-63-164
		Reactor 1	Reactor 2	
C_5-C_{10}	Non α-olefins	10.8	9.2	10.1
	α-olefins	16	19.9	21.4
	Non n-paraffins	5.1	8.4	6.1
	n-paraffins	5	5.9	6.0
	Aromatics	2.2	2	2.6
	Oxygenates	1.6	1.7	3.3
C_{11}-C_{22}	Non α-olefins	10.5	12.4	12.7
	α -olefins	20.7	18	17.1
	Non n-paraffins	9.5	5.9	5.8
	n-paraffins	7.8	5.8	5.4
	Aromatics	2.3	3	4.8
	Oxygenates	1.3	3.2	3.0
$>C_{22}$	Non α-olefins	1	0.6	0.4
	α-olefins	5.5	3.4	1.3
	Paraffins	0.7	0.6	0.0

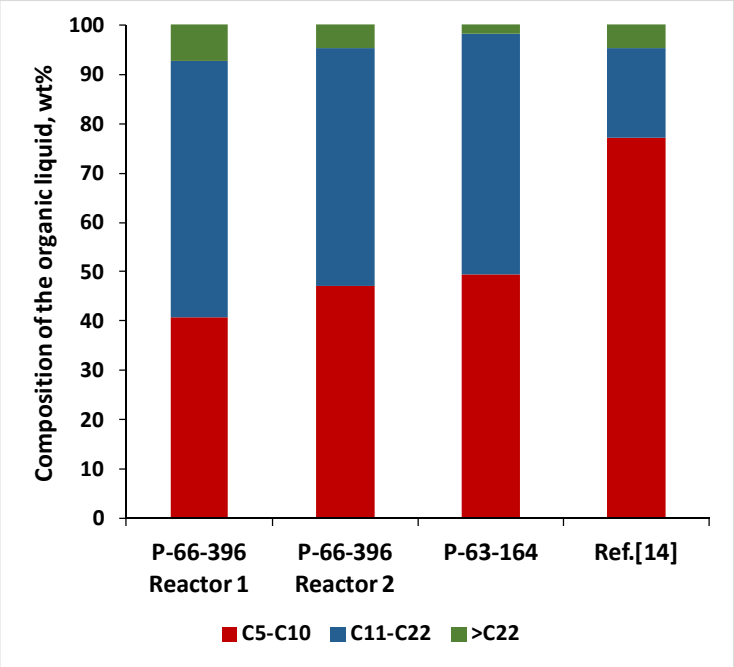

Fig. 7. A comparison of the liquid organic product between the first two reactors in run P-66-169, P-63-164 and Ref [14]. First reactor in P-66-169 is loaded with 3 wt% K, second reactor in P-66-169 is loaded with 4 wt% K. P-63-164 is loaded with 4 wt% K.

4. Conclusions

Potassium was found to be a key promoter that enhances significantly the reaction rates of RWGS and FTS and increases the selectivity to higher hydrocarbons while producing mostly olefins. The methanation rate was decreased extensively on the promoted catalysts. Those effects are a result of the lower hydrogenation activity, consistent with the observation of more reduced states of iron atoms at the spent steady state Fe-Al-O catalysts surface after addition of potassium. They could be attributed to the donation of electron density to vacant d-orbital of iron in both Fe-poor spinel and carbide phases thus enhancing the dissociative adsorption of CO while lowering the H_2 adsorption ability. The stabilization of Fe-poor spinel phase that prevented decomposition to magnetite phase contributed to the higher activity and selectivity of the catalyst. Furthermore, potassium enhanced the catalysts surface coverage with CO_2 as shown by CO_2-TPD data. The FTS reactions were accelerated by the enrichment of catalyst surface with carbide iron, especially more active Fe_5C_2 phase as established by the XRD and XPS data.

A detailed kinetic model was developed based on extensive experimental data. It includes the RWGS, methanation, 7 FTS, 4 oligomerization and oxygenates formation reactions. The fit of the kinetic model to the experimental data was very good. Specifically, the significant oligomerization activity of the catalyst that converts light olefins to higher hydrocarbons should be mentioned. Running mixtures of CO_2, CO and H_2 in the three reactor system packed with pelletized catalyst yielded a high productivity of higher hydrocarbons. The composition of the C_{5+} product was a function of the potassium content and the composition of the feed. A heavier product was measured with a catalyst containing 4 wt% potassium compared with the 3 wt% potassium catalyst and with a feed containing CO_2, CO and H_2 compared with a feed containing only CO_2 and H_2.

5. Acknowledgements

This work was supported by Israel - Strategic Alternative Energy Foundation (I-SAEF), the I-CORE Program of the Planning and Budgeting Committee and The Israel Science Foundation (grant No.152/11) and grant No. 582/13 of the Israel Science Foundation. The authors are grateful to Dr. A. Erenburg for XRD characterization of catalysts and to Dr. N. Froumin for characterization of catalysts by XPS.

6. References

1. World Energy Outlook, IEA, 12 November, 2014.
2. B. Friedrich, B. Schink, and R. K. Thauer, *Bioenergy- Chances and Limits*, German National Academy of Sciences Leopoldina, 2012, pp 1-118 (www.leopoldina.org).

3. F. Creutzig, C. von Stechow, D. Klein, C. Hunsberger, N. Bauer, A. Popp, and O. Edenhoferb, *Economics of Energy & Environmental Policy*, 2012, **1**, 65-82.
4. J. A. Herron, J. Kim, A. A. Upadhye, G. W. Huber and C. T. Maravelias, *Energy Environ. Sci*., 2015, **8**, 126–15.
5. G. Centi and S. Perathoner, *ChemSusChem*, 2010, **3**, 195 – 208.
6. K. S. Joya, Y. F. Joya, K. Ocakoglu, and R. van de Krol, *Angew. Chem. Int. Ed*., 2013, **52**, 10426 –10437.
7. B. A. Pinaud, J. D. Benck, L. C. Seitz, A. J. Forman, Z. Chen, T. G. Deutsch, B. D. James, K. N. Baum, G. N. Baum, S. Ardo, H. Wang, E. Millere and T. F. Jaramillo, *Energy Environ. Sci.*, 2013, **6**, 1983–2002.
8. J. R. McKone, N. S. Lewis, and H. B. Gray, *Chem. Mater.*, 2014, **26**, 407−414.
9. C. Agrafiotis, M. Roeb and C. Sattler, *Renewable and Sustainable Energy Reviews*, 2015, **42**, 254–285.
10. S. P.S. Badwal, S. Giddey and C. Munnings, *WIREs Energy Environ*, 2013, **2**, 473–487.
11. J. A. Trainham, J. Newman, C. A. Bonino, P. G. Hoertz and N. Akunuri, *Current Opinion in Chemical Engineering*, 2012, **1**, 204–210.
12. J. Newman, P. G. Hoertz, C. A. Bonino, and J. A. Trainham, *J. Electrochem. Soc.*, 2012, **159** (10) A1722-A1729.
13. C. Graves, S. D. Ebbesen, M. Mogensen and K. S. Lackner, *Renewable and Sustainable Energy Reviews*, 2011, **15**, 1–23.
14. M. V. Landau, R. Vidruk, and M. Herskowitz, *ChemSusChem*, 2014, **7**, 785-794.
15. D. A. Wood, C. Nwaoha and B. F. Towler, *J. Natural Gas Sci. and Eng.*, 2012, **9,** 196-208.
16. A. H. Lillebø, A. Holmen, B. C. Enger and E. A. Blekkan, *WIREs Energy Environ*, 2013, **2**, 507–524.
17. R. Rauch, J. Hrbek and H. Hofbauer, *WIREs Energy Environ* 2014, **3**, 343–362.
18. I. Hannula, *Biomass and Bioenergy* 2015, **74**, 26-46.
19. L. Yang, X. Ge, C. Wan, F. Yu and Y. Li, *Renewable and Sustainable Energy Reviews*, 2014, **40**, 1133–1152
20. S. C. Kang, K.-W. Jun and Y.-J. Lee, *Energy Fuels*, 2013, **27**, 6377−6387.
21. Y. Yao, X. Liu, D. Hildebrandt and D. Glasser, *Ind. Eng. Chem. Res.* 2011, **50**, 11002–11012.
22. M. V. Landau, R. Vidruk, and M. Herskowitz, WO Patent 2014111919, 2014.
23. J. Yang, W. Ma, D. Chen, A. Holmen and B. H. Davis, *Applied Catalysis A: General*, 2014, **470**, 250– 260.
24. M.-D. Lee, J.-F. Lee and C.-S. Chang, *Bull. Chem. Soc. Jpn.*, 1989, **62**, 2756-2758.
25. M. Martinelli, C. G. Visconti, L. Lietti, P. Forzatti, C. Bassano and P. Deiana, *Catalysis Today*, 2014, **228**, 77–88.
26. H. P. Bonzel, *Surf. Sci. Reports*, 1987, **8**, 43-125.

27. M. E. Dry, T. Shingles, L. J. Boshoff and G. J. Oostzuizen, *J. Catal.*, 1969, **15**, 190-199.
28. E. de Smit and B. M. Weckhuysen, *Chem. Soc. Rev.*, 2008, **37**, 2758-2781.
29. C. Zhang, K.-W. Jun, K.-S. Ha, Y.-J. Lee, and S. C. Kang, *Environ. Sci. Technol.*, 2014, 4**8**, 8251−8257.
30. T. Riedel, G. Schaub, K.-W. Jun and K.-W. Lee, *Ind. Eng. Chem. Res.* 2001**, 40**, 1355-1363.
31. M. Iglesias, C. de Vries, M. Claeys and G. Schaub, *Catalysis Today*, 2015, **242**, 184–192.
32. N. Park, J.-R. Kim, Y. Yoo, J. Lee and M.-J. Park, *Fuel*, 2014, **122**, 229–235.
33. M. E. Dry, *Catal.Today*, 1990, **6**, 183-206.
34. H. Wan, B. Wu, C. Zhang, H. Xiang and Y. Li, *J. Mol. Catal. A: Chemistry*, 2008, **283**, 33-42.
35. B. H. Davis, *Catal. Today*, 2009, **141**, 25-33.
36. J. B. Butt, *Catalysis Letters*, 1990, **7**, 61-82.
37. K. B. Sunil, , A. V. Anupama, B. Bikramjit and S. Balaram, *J. Phys. Chem. C*, 2015, **119**, 6539-6555.
38. http://xpssimplified.com/elements/carbon.php.
39. A. Furlan, U. Jansson, J. Lu, L. Hultman and M. Magnuson, L., *Phys. Condense Matter*, 2015, **27**, 045002 (9p).
40. X. An, B. Wu, H-J. Wan, T-Z. Li, Z-C. Tao, H-W. Xiang and Y-W. Li, *Catal. Commun.*, 2007, **8**, 1957-1962.